

Dynamics of Dark Pulse Affected by Higher-Order Effects in Microresonators

Wenmi Shi , Zhiheng Li, Xuening Fan, Qiyuan Sun, Mulong Liu , Huimin Huang , Zhizhou Lu, and Wei Zhao

Abstract—We theoretically investigate dynamics of dark pulse and Raman-Kerr microcombs generation influenced by higher-order effects, including high-order dispersion (HOD), stimulated Raman scattering (SRS) and self-steepening (SS) effects in silicon microresonators. These three effects cause the delay of dark pulse individually, or interact with each other to alter the drift velocity and direction of pulses. HOD effect can change pulse shift direction and even cause bifurcation. The temporal drift induced by SS or SRS effects could be balanced by the simultaneous third-order dispersion (TOD) engineering. In spectral domain, stable Raman-Kerr frequency comb will be generated due to the competition between strong SRS and Kerr effects. The Raman comb components are suppressed when HOD effect coexists, while SS effect has ignorable effect on the distribution of the Raman comb. Furthermore, the SS effect will increase the total energy of the spectrum by shifting the dispersive wave (DW) generation to the longer wavelength side. Our findings could deepen the understanding of intracavity nonlinear dynamics and provide theoretical guidance to precisely control the stabilization of dark pulse and the generation of broadband mid-infrared (MIR) microcomb.

Index Terms—Dark pulse, high-order dispersion, stimulated Raman scattering, self-steepening.

I. INTRODUCTION

MICRORESONATOR-BASED soliton microcombs have attracted significant interest among researchers due to their prospective applications in many fields, including high precision spectroscopy [1], [2], [3], coherent communication [4], [5], optical clocks [6], [7], microwave signal synthesis, imaging and ranging [8], [9], [10], [11]. This field are currently studied in two branches, namely bright and dark solitons generated in the anomalous group velocity dispersion (GVD) and the normal

group velocity dispersion regime, respectively. In particular, bright solitons have been explored actively in recent years and have been observed in many platforms like MgF_2 [12], [13], diamond [14], [15], silica [16], [17], aluminum nitride [18], silicon nitride [19], [20], [21], [22], [23], [24], [25], [26], and silicon [27], [28] microresonators, achieved by elaborate waveguide cross-section engineering. Actually, many optical materials present normal GVD in the visible and near-infrared range due to ultraviolet absorption, which makes it still challenging to obtain anomalous dispersion at arbitrary center wavelengths [26]. What's more, dark pulses are more efficient than bright solitons sequences for the same absolute value of anomalous GVD in terms of the pump-to-comb conversion [29], [30]. Excitation of dark pulse in the normal GVD can also increase the degree of freedom in the design and fabrication of microresonators, thus enabling access to microcombs generation in more materials and extended wavelength ranges. Furthermore, compared with their anomalous dispersion-based counterpart, the generation of dark pulse is also more stable due to the avoidance of chaotic and multi-soliton states [31].

To date, dark pulses have been observed experimentally in silica [32], AlN [33], [34], Ge [35], [36], [37], and Si_3N_4 [38], [39], [40] microresonators with normal GVD. Extensive techniques have been introduced for their excitation, including mode coupling [41], [42], self-injection locking [43], [44], [45], negative thermal effects [46], free carrier effects [47], bichromatic or amplitude-modulated pump schemes [29], [48]. In general, the dark pulse microcombs currently are mainly studied in the communication band. Silicon has a high nonlinear coefficient and a wide transparent window, as an excellent platform for generation of microcombs in the MIR. The MIR band is the fingerprint region of many gas molecules (e.g., pollutants and greenhouse gases) [49], [50], and the high conversion efficiency of dark pulse could provide an effective support for MIR spectroscopy. However, reports on silicon microresonators with normal GVD are limited. The influences of TOD and SRS effects on dark pulse have been solely investigated. TOD induces the temporal drift of dark pulse [41], [51], SRS causes strong instabilities of dark pulse associated with the Kerr effect [52]. In addition, SS effect within the cavity also impose non-negligible influences on pulse stability and spectral bandwidth while its role in microresonators still remain unrevealed. Due to complex dynamic processes within the microcavity, the threshold of complexity and non-linear effects within Arnold tongues in Kerr microresonators is studied [53]. Higher-order effects such as HOD, SRS, and SS effects generally exist simultaneously, and the interaction

Manuscript received 12 September 2022; revised 29 October 2022; accepted 1 December 2022. Date of publication 7 December 2022; date of current version 4 January 2023. This work was supported in part by the Natural Science Basic Research Program of Shaanxi under Grants 2022JQ-066 and 2022JQ-688, and in part by the National Natural Science Foundation of China under Grants 52002331 and 12204381. (*Corresponding authors:* Mulong Liu; Huimin Huang.)

Wenmi Shi, Zhiheng Li, Xuening Fan, Qiyuan Sun, and Mulong Liu are with the Institute for School of Science, Northwest A&F University, Yangling 712100, China (e-mail: 15650522088@163.com; zhihengli@nwafu.edu.cn; dupre663@163.com; sunyuan3309507@163.com; lingshu@nwafu.edu.cn).

Huimin Huang is with the Institute for College of Information Engineering, Northwest A&F University, Yangling 712100, China (e-mail: huanghm@nwafu.edu.cn).

Zhizhou Lu is with the Institute for Chongqing United Microelectronics Center, Chongqing 401332, China (e-mail: luzhizhou1992@126.com).

Wei Zhao is with the Institute for State Key Laboratory of Transient Optics and Photonics, Xi'an Institute of Optics and Precision Mechanics, Chinese Academy of Sciences, Xi'an 710119, China (e-mail: weiz@opt.ac.cn).

Digital Object Identifier 10.1109/JPHOT.2022.3227173

mechanism among them has not been reported. Studying the interaction of these effects contributes to further control the stabilization of dark pulses and their spectral bandwidths.

In this work, we theoretically investigate the dynamics of dark pulse and the generation of Raman-Kerr microcombs in silicon microresonators with normal GVD in the presence of HOD, SRS and SS effects. It is found that higher-order effects can cause pulse bifurcation and drift direction changes. HOD effect attenuates the temporal shift and perturbation caused by SRS effect, while drift velocity increases significantly when HOD and SS effects exist simultaneously. Pulse delay associated with the SS or SRS effects can be balanced by TOD design. In spectral domain, strong SRS effect competes with the Kerr effect during the four-wave mixing (FWM) process, eventually resulting in stable Raman-Kerr frequency comb that reach equilibrium. Raman comb components and spectral broadening due to SRS effect can be suppressed by HOD effect but are less affected by SS effect. It is revealed that SS effect will shift the generation position of the DW to the longer wavelength side and thus enhance the total energy of spectrum. These studies are important theoretical complements to the dynamics of dark pulse and the generation of Raman-Kerr microcombs, not only providing novel ideas for the further stabilization of dark pulse, but also contributing to the acquisition of broadband MIR microcomb.

II. THEORETICAL MODEL

In order to model the physical process in normal dispersion silicon microresonators, the modified Lugiato-Lefever equation (LLE) including HOD, three-photon absorption (3PA), free-carrier (FC), SS and SRS effects is used to describe the spectral-temporal dynamics of frequency combs [54]. This model is a variant of the nonlinear Schrödinger equation widely used to describe nonlinear effects in pulse transmission [55], [56], [57], [58].

$$\begin{aligned} T_R \frac{\partial E(t, \tau)}{\partial t} = & \left[-\frac{\alpha}{2} - \frac{\kappa}{2} - i\delta_0 + iL \sum_{n \geq 2} \frac{\beta_n}{n!} \left(i \frac{\partial}{\partial \tau} \right)^n \right. \\ & + \left(1 + \frac{i}{\omega_0} \frac{\partial}{\partial \tau} \right) \times \left(\int_0^\infty R(t') |E(t-t', \tau)|^2 dt' \right. \\ & \left. \left. - \frac{\beta_{3PA} L}{3A_{eff}^2} |E(t, \tau)|^4 \right) \right. \\ & \left. - \frac{\sigma L}{2} (1 + i\mu) \langle N_c(t, \tau) \rangle \right] E(t, \tau) \\ & + \sqrt{\kappa E_{in}}, \end{aligned} \quad (1)$$

$$\frac{d \langle N_c(t) \rangle}{dt} = \frac{\beta_{3PA}}{3\hbar\omega} \frac{\langle |E|^6 \rangle}{A_{eff}^3} - \frac{\langle N_c(t) \rangle}{\tau_{eff}}, \quad (2)$$

$$H_R(\Omega) = \frac{\Omega_R^2}{\Omega_R^2 - \Omega^2 - 2i\Gamma_R\Omega}, \quad (3)$$

where $E(t, \tau)$ is the field in the resonator, t and τ correspond to the slow and fast time, respectively, T_R is the round-trip time, L is the total cavity length, α is the round-trip loss, κ

is the power transmission coefficient between bus-waveguide and microresonator. δ_0 is the cavity detuning, β_n is the n-th order dispersion parameter, γ is the nonlinear coefficient, $R(t)$ is the Raman response, β_{3PA} is the three-photon absorption coefficient, σ is the free-carrier absorption (FCA) cross-section and μ is the free-carrier dispersion (FCD) parameter. E_{in} is the pump field. The term contains i/ω_0 is related to SS effect. In (2), the averaged FC density $\langle N_c(t) \rangle = (1/T_R) \int_{-T_R/2}^{T_R/2} N(t, \tau) d\tau$ describes the buildup of carriers within the cavity over successive round trips [29]. Free-carrier generation is governed by 3PA and the recombination rate is determined by the effective FC lifetime τ_{eff} , which can be controlled by a positive intrinsic negative (PIN) diode and is set as 5 ps [59], [60]. Here, single pump combining with the pump mode eigenfrequency shifted is adopted [52]. The Raman effect is calculated by the convolution theorem which states $R(t) \otimes |E(t, \tau)|^2 = \mathcal{F}^{(-1)}(\mathcal{F}[R(t)] \cdot \mathcal{F}[|E(t, \tau)|^2])$. The Fourier transform of the Raman response used here is a Lorentzian gain spectrum in the form of (3), where the full width at half maximum (FWHM) of Raman gain spectrum is $\Gamma_R/\pi = 105$ GHz at room temperature and the peak gain frequency shift $\Omega_R/2\pi = 15.6$ THz. The Raman part of the material susceptibility in the classical approximation can also be described by the oscillator equation, which allows a straightforward theoretical study of instabilities as done in [61].

III. THE INFLUENCE OF HOD, SRS AND SS ON DARK PULSE, RESPECTIVELY

We first consider the dark pulse generation in silicon microresonators with only Kerr effect. A dual-pulse can be excited with mode-coupling method as shown in Fig. 1, where the pump detuning is kept at fixed value of 0.065 after 30 ns. Fig. 1(a)-(b) show the temporal and spectral profiles of the generated dark pulse exhibiting a two-soliton-like property as in the anomalous dispersion regime. Such pulses can stably evolve in the cavity as can be seen from the temporal evolution [Fig. 1(c)] and its energy evolution diagram [Fig. 1(d)]. While dark pulses are largely affected by higher-order effects, including HOD, SRS and SS effects. Fig. 2 shows the spatiotemporal results with HOD [Fig. 2(a)-(c)], SRS [Fig. 2(d)-(f)] and SS [Fig. 2(g)-(i)] effects, respectively. Obviously, the dark pulses in all three cases reduce in number and present different degrees of inclination compared to the case of only Kerr effect [see Figs. 1(c), 2(c), (f) and (i)], indicating that these three effects can solely break the nonlinear symmetry of the localized structures interaction and cause temporal drift of dark pulses.

In detail, dark pulses have asymmetric bilateral oscillatory tails and weak top oscillations with HOD [Fig. 2(a)]. The breaking of nonlinear symmetry in time domain is mainly due to the DW introduced by the HOD effect through the Cerenkov radiation (CR) process. Emission of the DW will induce the spectral recoil on the soliton core shifting the soliton carrier frequency away from the zero group-velocity dispersion (GVD) point. Theoretically, the drift direction and velocity of dark pulses mainly depends on the sign and amplitude of TOD and the detuning [62]. The phase-matching condition governing the

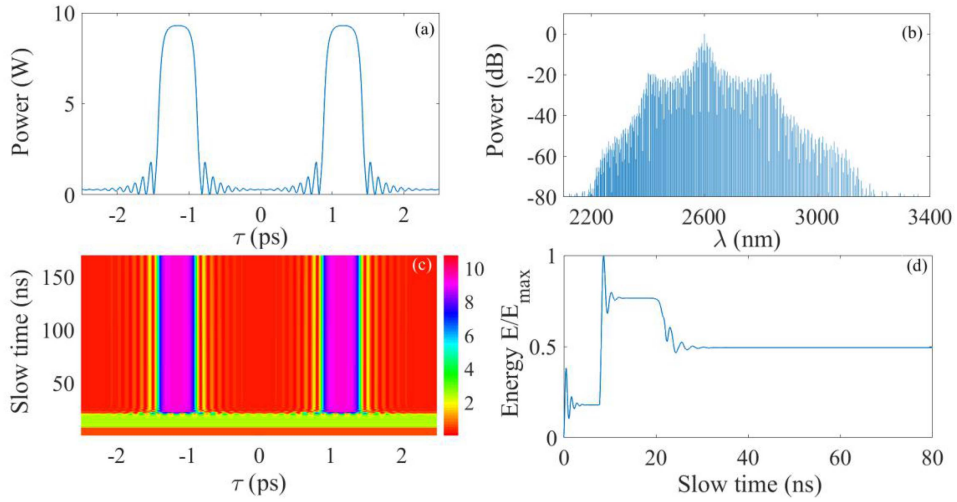


Fig. 1. Temporal (a) and spectral (b) profiles of dark pulses in one cycle, (c) temporal evolution of dark pulses, (d) intracavity energy evolution of (c) with only Kerr effect.

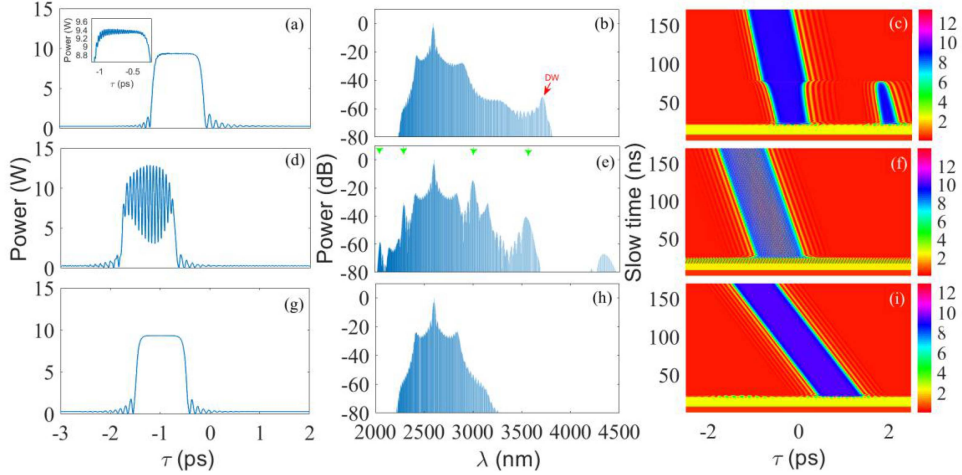


Fig. 2. Influences of three higher-order effects on dark pulses. Left to right: temporal profiles, spectral profiles and temporal evolution with only HOD effect (a)–(c), SRS effect (d)–(f), and SS effect (g)–(i), respectively. The inset in (a) shows the weakly top oscillating field. The location of DW and Raman frequency shift are marked with red (b) and green (e) arrows, respectively.

resonant DW via CR is [31],

$$\beta(\omega_{DW}) - \beta_1(\omega_S)\omega_{DW} = \beta(\omega_S) - \beta_1(\omega_S)\omega_S, \quad (4)$$

where ω_{DW} and ω_S are the central angular frequencies of the DW and the dark pulses, respectively [31]. The location of DW is marked with red arrows in Fig. 2(b). The strong and narrow Raman gain in silicon microresonators exerts different influence on dark pulse. The energy balance is among drive, loss and the intra-pulse Raman scattering induced pulse energy transfer. The dark pulse profile is consequently distorted and reveals some new spectral components located at specific wavelengths around the pump. Crystalline materials (e.g., Silicon) with narrow Raman gain bandwidths typically exhibit negligible Raman self-frequency shift. SRS can interfere the FWM process and thus perturbing the temporal and spectral profiles distribution of dark pulse [Fig. 2(d) and (e)]. Although the temporal intensity shows violent oscillation and the spectrum contain Raman comb

components, the generated pulse can keep shape-invariant over slow time [Fig. 2(f)], indicating that the competition of SRS effect and FWM process eventually reaches equilibrium. The Raman frequency components at wavelengths of 2046 nm, 2290 nm, 3006 nm, and 3563 nm, are marked by green arrows [Fig. 2(e)]. As for SS effect, the pulse trailing edge becomes steeper thus resulting in intracavity drift [Fig. 2(i)]. In spectral domain, HOD and SRS effects will broaden the bandwidth obviously, while SS effect hardly changes the spectral width [compare Figs. 2(b), (e), (h) and 1(c)].

IV. THE INTERACTION BETWEEN HOD, RAMAN AND SS EFFECTS

Physically, these higher-order effects often exist simultaneously in microcavities, but their interaction have not yet been revealed. In order to study the interaction between SRS and

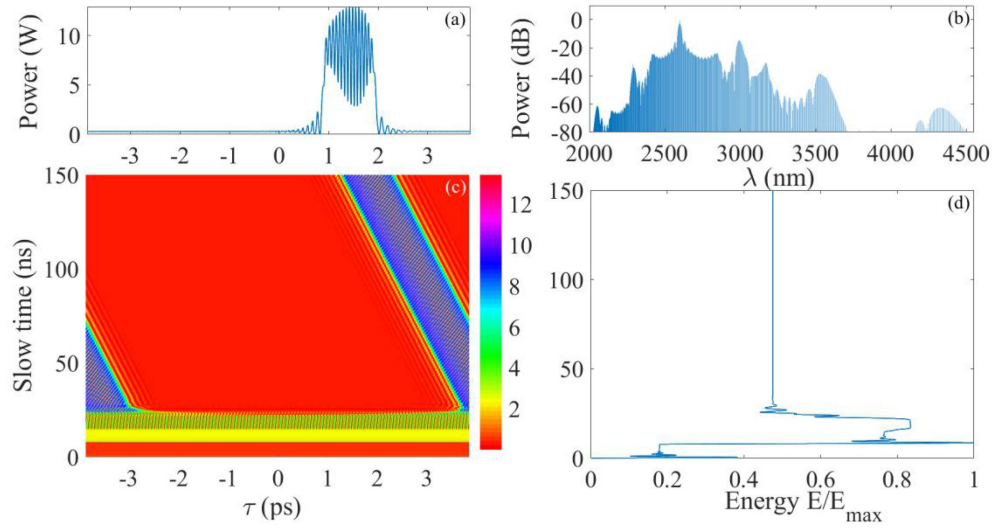


Fig. 3. Temporal (a) and spectral (b) profiles of dark pulse in one cycle, (c) temporal evolution, (d) intracavity energy evolution of (c) with SRS and SS effects considered.

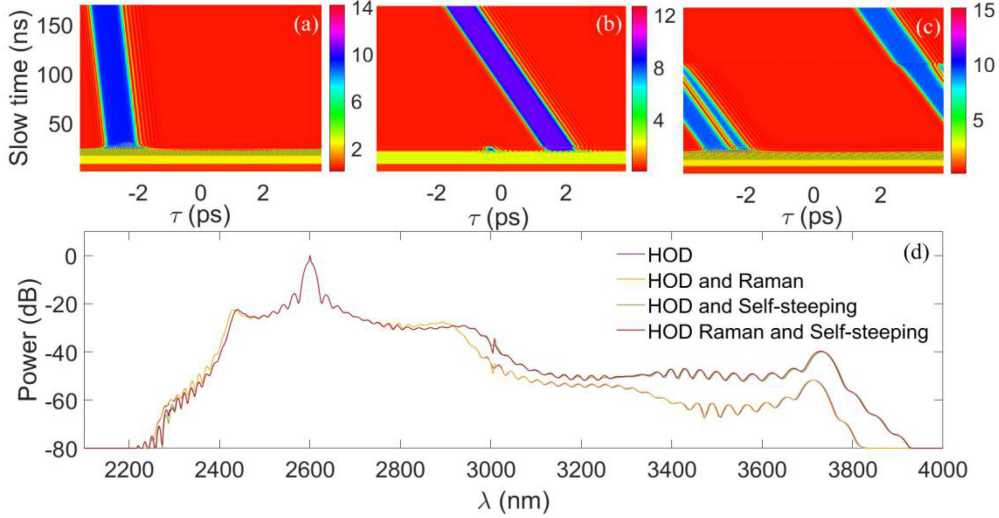


Fig. 4. Temporal evolution of dark pulses under the interaction of HOD and SRS effects (a), HOD and SS effects (b), and all three higher-order effects (c). (d) Corresponding spectral profiles with HOD (purple), HOD and SRS (yellow), HOD and SS (green), and all three higher-order effects (red).

SS effects, we set HOD terms as 0 and the results shown in Fig. 3 are obtained. Obviously, the temporal profile also shows a severe top oscillation [Fig. 3(a)] and the spectrum is broadened [Fig. 3(b)] due to SRS effect, which means that SS effect has ignorable effect on the distribution of Raman comb components. In addition, the increased SS effect also intensifies the drift of pulse [compare Figs. 3(c) and 2(f)]. To illustrate the additional velocity of the dark pulse envelope in time domain in detail, the slope is described by k (fs/ns). Specifically, k is 0 for the dark pulses in Fig. 1(c) (only Kerr), while it is equal to -3.51 , -5.81 and -12.99 in Fig. 2(c), (f) and (i) (only HOD, SRS or SS), respectively. The situation becomes different when interaction between higher-order effects is considered in the system. Fig. 4(a)-(c) depict the temporal evolution of dark pulses, in

which the corresponding k values are -3.58 (HOD and SRS), -21.25 (HOD and SS), and -20.90 (all three) in turn. It can be seen from the comparison that the temporal drift of dark pulse perturbed by SRS effect can be weakened by HOD effect [Figs. 2(f) and 4(a)], while the simultaneous existence of SS effect will apparently enhance the temporal drift due to HOD effect [Figs. 2(c) and 4(b)]. One can also observe bifurcation in Figs. 2(c) and 4(c). Dark pulses are naturally formed by interlocked switching waves (SWs) or fronts connecting the high and low homogeneous steady solutions of the bistable systems. SWs connecting the top and bottom branches can lock around the Maxwell point with certain pulse width [63]. Since dark pulses are formed by binding of two counter-propagating SWs, the bifurcation discussed here results from different relative

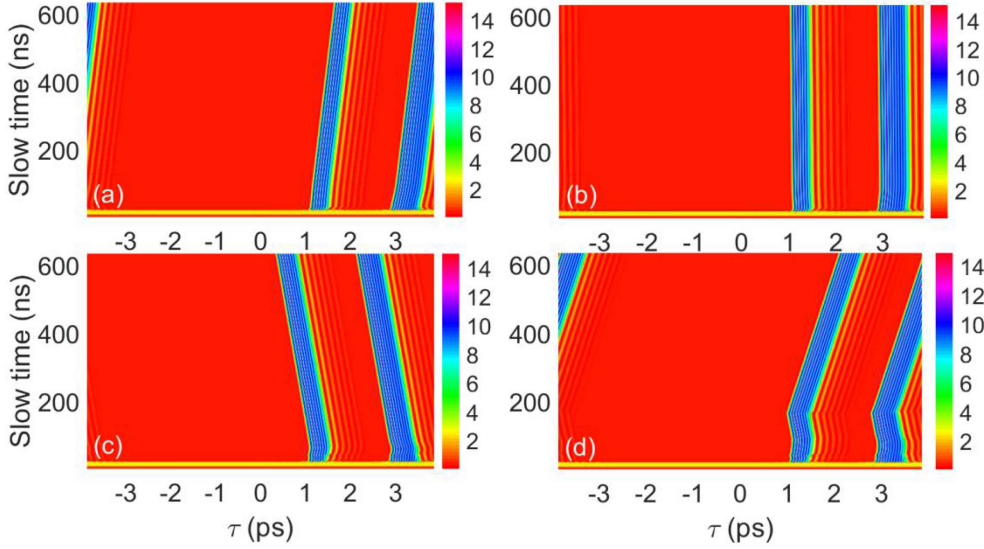


Fig. 5. Results of TOD effect on temporal properties of dark pulses in the presence of SS effect. Temporal evolution for the conditions of (a) $\beta_3 = 2.137 \text{ ps}^3/\text{km}$, (b) $\beta_3 = 2.128 \text{ ps}^3/\text{km}$, (c) $\beta_3 = 2.097 \text{ ps}^3/\text{km}$ and (d) $\beta_3 = 2.094 \text{ ps}^3/\text{km}$.

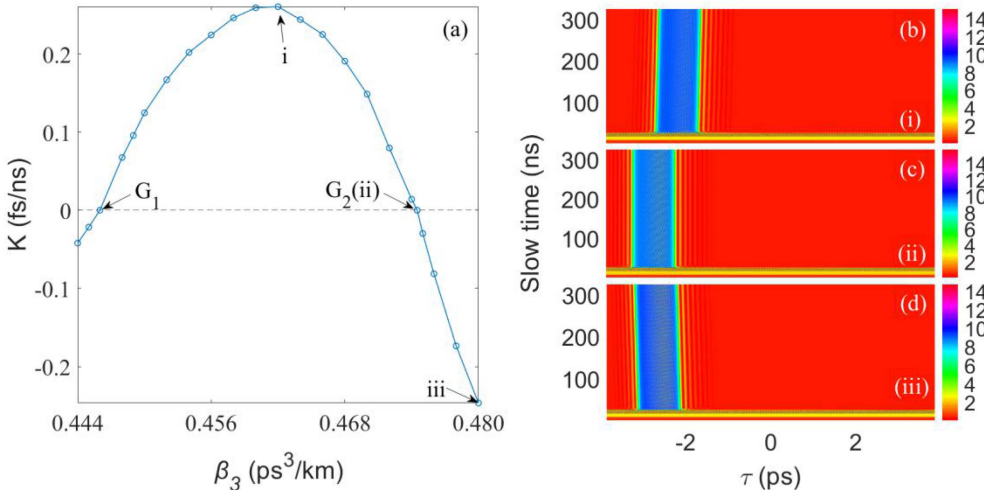


Fig. 6. Results of TOD effect on the temporal properties of dark pulses in the presence of SRS effect. (a) Slope plot of temporal evolution under different β_3 where points i and ii are two zeros of (a). Temporal evolution at points i (b), ii (c) and iii (d) in (a) under the conditions of $\beta_3 = 0.462 \text{ ps}^3/\text{km}$, $\beta_3 = 0.474 \text{ ps}^3/\text{km}$, $\beta_3 = 0.480 \text{ ps}^3/\text{km}$, respectively.

velocities of these fronts caused by higher-order effects, which frustrates robustness of dark pulses. Their spectra are given in Fig. 4(d). The Raman frequency comb components and the broadening effect of SRS effect (shown in Fig. 2(e)) will be suppressed by HOD effect as the spectral profiles without (purple curve in Fig. 4(d)) and with SRS effect (yellow curve in Fig. 4(d)) are roughly coincided in the bandwidth. Furthermore, SS effect can also broaden the spectral range of the frequency combs in the presence of HOD effect, since the spectrum with SS effect (red curve in Fig. 4(d)) is wider than that without SS effect (yellow curve in Fig. 4(d)) after 3800 nm (also seen by comparing green curve with purple curve). Meanwhile, SS effect changes the position of the DW, moving it towards the longer wavelength and thus increasing the energy of the spectrum.

V. THE BALANCE OF PULSE DRIFT WITH TOD

In this section, the possibility of balancing the pulse drift induced by TOD, SS and SRS effects is investigated. As discussed above, higher-order effects can individually cause temporal drift. Especially, the temporal drift caused by HOD mainly depends on the sign and amplitude of TOD values [41]. Here, TOD effect is considered to balance such delay introduced by SS or SRS effects in simulations. Fig. 5(a)-(d) show the temporal evolution with same SS while different TOD coefficient β_3 (ps^3/km). Specifically, the pulses in Fig. 5(a) and (c) drift in opposite directions and they are split into two parts with a larger β_3 . Thus the pulse evolves without any temporal drift if a suitable β_3 is taken into account, as shown in Fig. 5(b). This means

that TOD balances the temporal drift caused by SS effect of the dark pulse. In addition, dark pulse in Fig. 5(d) undergoes a turning point during evolution due to the influence of the added TOD.

Besides SS effect, the temporal drift of dark pulse resulted from SRS effect can also be balanced by TOD. An exact balance between the DW-induced spectral recoil and the Raman effect can cause the existence of a quiescent soliton [61]. To illustrate, a more detailed image about pulse drift velocity due to the interaction of TOD and SRS effects is shown in Fig. 6(a). Fig. 6(b)-(d) depict the temporal evolution at points i, ii and iii in Fig. 6(a), respectively. It can be observed in Fig. 6(a) that there is a parabolic-like relationship between k and β_3 . As the increase of β_3 , the drift direction and velocity of dark pulses varies since k first changes from negative to positive, and then starts to decrease after β_3 exceeds 0.462. In particular, there are two equilibrium points G_1 and G_2 (values of β_3 are 0.446 and 0.474, respectively), where the drift of the pulse will vanish (see Fig. 6(c)). This means that the direction and magnitude of the pulse drift caused by SRS effect can also be modulated by TOD effect, just like the pulse drift by SS effect. TOD effect has a regular influence on the pulse delay caused by SRS effect, and we found two β_3 values where the pulse drift is balanced out. Overall, these results indicate that different TOD will result in different drift directions, drift velocities and pulse shapes in time domain.

VI. CONCLUSION

In conclusion, dark pulse dynamics and Raman-Kerr microcombs generation in silicon microresonators affected by higher-order effects are investigated theoretically. In time domain, HOD effect can introduce changes of pulse drift direction or even bifurcation. Temporal drift caused by SS or SRS effects could be balanced by the design of TOD effect. In spectral domain, strong SRS effect competes with Kerr effect, resulting in stable Raman-Kerr frequency comb. Raman comb components and spectral broadening of SRS effect are suppressed by the HOD effect but are slightly influenced by the SS effect. The SS effect increases the total energy of the spectrum by shifting the DW generation to the longer wavelength side. These studies provide new ideas for stabilizing of dark pulse, and also facilitate the acquisition of stable broadband microcomb in the MIR. Our work could also constitute supplements to deeper the understanding of impact of higher-order effects and their interaction dynamics.

REFERENCES

- [1] L. Stern et al., “Direct Kerr frequency comb atomic spectroscopy and stabilization,” *Sci. Adv.*, vol. 6, 2020, Art. no. eaax6230.
- [2] Q.-F. Yang et al., “Vernier spectrometer using counterpropagating soliton microcombs,” *Science*, vol. 363, pp. 965–968, 2019.
- [3] A. Dutt et al., “On-chip dual-comb source for spectroscopy,” *Sci. Adv.*, vol. 4, 2018, Art. no. e1701858.
- [4] B. Corcoran et al., “Ultra-dense optical data transmission over standard fibre with a single chip source,” *Nature Commun.*, vol. 11, pp. 1–7, 2020.
- [5] A. Fülop et al., “High-order coherent communications using mode-locked dark-pulse Kerr combs from microresonators,” *Nature Commun.*, vol. 9, pp. 1–8, 2018.
- [6] Z. L. Newman et al., “Architecture for the photonic integration of an optical atomic clock,” *Optica*, vol. 6, pp. 680–685, 2019.
- [7] Z. Newman et al., “Architecture for the photonic integration of an optical atomic clock,” *Optica*, vol. 6, pp. 680–685, 2019.
- [8] J. Riemenberger et al., “Massively parallel coherent laser ranging using a soliton microcomb,” *Nature*, vol. 581, pp. 164–170, 2020.
- [9] W. Wang, L. Wang, and W. Zhang, “Advances in soliton microcomb generation,” *Adv. Photon.*, vol. 2, 2020, Art. no. 034001.
- [10] M.-G. Suh and K. J. Vahala, “Soliton microcomb range measurement,” *Science*, vol. 359, pp. 884–887, 2018.
- [11] P. Trocha et al., “Ultrafast optical ranging using microresonator soliton frequency combs,” *Science*, vol. 359, pp. 887–891, 2018.
- [12] E. Lucas, P. Brochard, R. Bouchand, S. Schilt, T. Südmeyer, and T. J. Kippenberg, “Ultralow-noise photonic microwave synthesis using a soliton microcomb-based transfer oscillator,” *Nature Commun.*, vol. 11, pp. 1–8, 2020.
- [13] E. Lucas et al., “Spatial multiplexing of soliton microcombs,” *Nature Photon.*, vol. 12, pp. 699–705, 2018.
- [14] G. Lin and Q. Song, “Kerr frequency comb interaction with Raman, Brillouin, and second order nonlinear effects,” *Laser Photon. Rev.*, vol. 16, 2022, Art. no. 2100184.
- [15] Y. Okawachi et al., “Competition between Raman and Kerr effects in microresonator comb generation,” *Opt. Lett.*, vol. 42, pp. 2786–2789, 2017.
- [16] H.-J. Chen et al., “Chaos-assisted two-octave-spanning microcombs,” *Nature Commun.*, vol. 11, pp. 1–6, 2020.
- [17] F. X. Wang et al., “Quantum key distribution with on-chip dissipative Kerr soliton,” *Laser Photon. Rev.*, vol. 14, 2020, Art. no. 1900190.
- [18] H. Jung, R. Stoll, X. Guo, D. Fischer, and H. X. Tang, “Green, red, and IR frequency comb line generation from single IR pump in AlN microring resonator,” *Optica*, vol. 1, pp. 396–399, 2014.
- [19] J. Hu et al., “Photo-induced cascaded harmonic and comb generation in silicon nitride microresonators,” *Sci. Adv.*, vol. 8, 2022, Art. no. eadd8252.
- [20] J. Liu et al., “High-yield, wafer-scale fabrication of ultralow-loss, dispersion-engineered silicon nitride photonic circuits,” *Nature Commun.*, vol. 12, pp. 1–9, 2021.
- [21] C. Xiang et al., “Laser soliton microcombs heterogeneously integrated on silicon,” *Science*, vol. 373, pp. 99–103, 2021.
- [22] X. Ji et al., “Exploiting ultralow loss multimode waveguides for broadband frequency combs,” *Laser Photon. Rev.*, vol. 15, 2021, Art. no. 2000353.
- [23] B. Shen et al., “Integrated turnkey soliton microcombs,” *Nature*, vol. 582, pp. 365–369, 2020.
- [24] Z. Ye, K. Twayana, and P. A. Andrekson, “High-Q Si₃N₄ microresonators based on a subtractive processing for Kerr nonlinear optics,” *Opt. Exp.*, vol. 27, pp. 35719–35727, 2019.
- [25] T. J. Kippenberg, A. L. Gaeta, M. Lipson, and M. L. Gorodetsky, “Dissipative Kerr solitons in optical microresonators,” *Science*, vol. 361, 2018, Art. no. eaan8083.
- [26] M. Karpov, M. H. Pfeiffer, J. Liu, A. Lukashchuk, and T. J. Kippenberg, “Photonic chip-based soliton frequency combs covering the biological imaging window,” *Nature Commun.*, vol. 9, pp. 1–8, 2018.
- [27] M. Yu, Y. Okawachi, A. G. Griffith, N. Picqué, M. Lipson, and A. L. Gaeta, “Silicon-chip-based mid-infrared dual-comb spectroscopy,” *Nature Commun.*, vol. 9, pp. 1–6, 2018.
- [28] M. Yu, Y. Okawachi, A. G. Griffith, M. Lipson, and A. L. Gaeta, “Mode-locked mid-infrared frequency combs in a silicon microresonator,” *Optica*, vol. 3, pp. 854–860, 2016.
- [29] M. Liu et al., “Influences of multiphoton absorption and free-carrier effects on frequency-comb generation in normal dispersion silicon microresonators,” *Photon. Res.*, vol. 6, pp. 238–243, 2018.
- [30] X. Xue, P. H. Wang, Y. Xuan, M. Qi, and A. M. Weiner, “Microresonator Kerr frequency combs with high conversion efficiency,” *Laser Photon. Rev.*, vol. 11, 2017, Art. no. 1600276.
- [31] M. Liu, H. Huang, Z. Lu, Y. Wang, Y. Cai, and W. Zhao, “Dynamics of dark breathers and Raman-Kerr frequency combs influenced by high-order dispersion,” *Opt. Exp.*, vol. 29, pp. 18095–18107, 2021.
- [32] D. Yoon Oh, K. Y. Yang, C. Fredrick, G. Ycas, S. A. Diddams, and K. J. Vahala, “Coherent ultra-violet to near-infrared generation in silica ridge waveguides,” *Nature Commun.*, vol. 8, pp. 1–7, 2017.
- [33] Z. Gong et al., “High-fidelity cavity soliton generation in crystalline AlN micro-ring resonators,” *Opt. Lett.*, vol. 43, pp. 4366–4369, 2018.
- [34] D. D. Hickstein et al., “Ultrabroadband supercontinuum generation and frequency-comb stabilization using on-chip waveguides with both cubic and quadratic nonlinearities,” *Phys. Rev. Appl.*, vol. 8, 2017, Art. no. 014025.
- [35] R. Guo, W. Chen, H. Gao, Y. Zhao, T. Liu, and Z. Cheng, “Is Ge an excellent material for mid-IR Kerr frequency combs around 3-μm wavelengths?”, *J. Lightw. Technol.*, vol. 40, no. 7, pp. 2097–2103, Apr. 2022.

- [36] M. Liu et al., "Stimulated Raman scattering induced dark pulse and microcomb generation in the mid-infrared," *New J. Phys.*, vol. 24, 2022, Art. no. 053003.
- [37] Y. Guo et al., "Power-efficient generation of two-octave mid-IR frequency combs in a germanium microresonator," *Nanophotonics*, vol. 7, pp. 1461–1467, 2018.
- [38] H. Tian et al., "Magnetic-free silicon nitride integrated optical isolator," *Nature Photon.*, vol. 15, pp. 828–836, 2021.
- [39] D. Martyshkin et al., "Visible-near-middle infrared spanning supercontinuum generation in a silicon nitride (Si_3N_4) waveguide," *Opt. Mater. Exp.*, vol. 9, pp. 2553–2559, 2019.
- [40] H. Guo et al., "Mid-infrared frequency comb via coherent dispersive wave generation in silicon nitride nanophotonic waveguides," *Nature Photon.*, vol. 12, pp. 330–335, 2018.
- [41] V. E. Lobanov, A. V. Cherenkov, A. E. Shitikov, I. A. Bilenko, and M. L. Gorodetsky, "Dynamics of platicons due to third-order dispersion," *Eur. Phys. J. D*, vol. 71, pp. 1–5, 2017.
- [42] J. K. Jang et al., "Dynamics of mode-coupling-induced microresonator frequency combs in normal dispersion," *Opt. Exp.*, vol. 24, pp. 28794–28803, 2016.
- [43] G. Lihachev et al., "Platicon microcomb generation using laser self-injection locking," *Nature Commun.*, vol. 13, pp. 1–9, 2022.
- [44] W. Jin et al., "Hertz-linewidth semiconductor lasers using CMOS-ready ultra-high-Q microresonators," *Nature Photon.*, vol. 15, pp. 346–353, 2021.
- [45] N. M. Kondratiev, V. E. Lobanov, E. A. Lonshakov, N. Y. Dmitriev, A. S. Voloshin, and I. A. Bilenko, "Numerical study of solitonic pulse generation in the self-injection locking regime at normal and anomalous group velocity dispersion," *Opt. Exp.*, vol. 28, pp. 38892–38906, 2020.
- [46] V. E. Lobanov, N. M. Kondratiev, and I. A. Bilenko, "Thermally induced generation of platicons in optical microresonators," *Opt. Lett.*, vol. 46, pp. 2380–2383, 2021.
- [47] M. Liu et al., "Free carrier induced dark pulse generation in microresonators," *Opt. Lett.*, vol. 46, pp. 4462–4465, 2021.
- [48] V. E. Lobanov, N. M. Kondratiev, A. E. Shitikov, R. R. Galiev, and I. A. Bilenko, "Generation and dynamics of solitonic pulses due to pump amplitude modulation at normal group-velocity dispersion," *Phys. Rev. A*, vol. 100, 2019, Art. no. 013807.
- [49] T. Butler et al., "Watt-scale 50-MHz source of single-cycle waveform-stable pulses in the molecular fingerprint region," *Opt. Lett.*, vol. 44, pp. 1730–1733, 2019.
- [50] C. Gaida et al., "Watt-scale super-octave mid-infrared intrapulse difference frequency generation," *Light: Sci. Appl.*, vol. 7, pp. 1–8, 2018.
- [51] M. Liu et al., "Influences of high-order dispersion on temporal and spectral properties of microcavity solitons," *Opt. Exp.*, vol. 26, pp. 16477–16487, 2018.
- [52] A. Cherenkov, N. Kondratiev, V. Lobanov, A. Shitikov, D. Skryabin, and M. Gorodetsky, "Raman-Kerr frequency combs in microresonators with normal dispersion," *Opt. Exp.*, vol. 25, pp. 31148–31158, 2017.
- [53] D. Skryabin, Z. Fan, A. Villois, and D. Puzyrev, "Threshold of complexity and Arnold tongues in Kerr-ring microresonators," *Phys. Rev. A*, vol. 103, 2021, Art. no. L011502.
- [54] T. Hansson, D. Modotto, and S. Wabnitz, "Mid-infrared soliton and Raman frequency comb generation in silicon microrings," *Opt. Lett.*, vol. 39, pp. 6747–6750, 2014.
- [55] Y. Fang, G.-Z. Wu, X.-K. Wen, Y.-Y. Wang, and C.-Q. Dai, "Predicting certain vector optical solitons via the conservation-law deep-learning method," *Opt. Laser Technol.*, vol. 155, 2022, Art. no. 108428.
- [56] R.-R. Wang, Y.-Y. Wang, and C.-Q. Dai, "Influence of higher-order nonlinear effects on optical solitons of the complex Swift-Hohenberg model in the mode-locked fiber laser," *Opt. Laser Technol.*, vol. 152, 2022, Art. no. 108103.
- [57] X.-K. Wen, G.-Z. Wu, W. Liu, and C.-Q. Dai, "Dynamics of diverse data-driven solitons for the three-component coupled nonlinear Schrödinger model by the MPS-PINN method," *Nonlinear Dyn.*, vol. 109, pp. 3041–3050, 2022.
- [58] B. Wang, H. Han, L. Yu, Y. Wang, and C. Dai, "Generation and dynamics of soliton and soliton molecules from a VSe₂/GO-based fiber laser," *Nanophotonics*, vol. 11, pp. 129–137, 2022.
- [59] A. G. Griffith et al., "Coherent mid-infrared frequency combs in silicon-microresonators in the presence of Raman effects," *Opt. Exp.*, vol. 24, pp. 13044–13050, 2016.
- [60] A. C. Turner-Foster et al., "Ultrashort free-carrier lifetime in low-loss silicon nanowaveguides," *Opt. Exp.*, vol. 18, pp. 3582–3591, 2010.
- [61] C. Milián, A. V. Gorbach, M. Taki, A. V. Yulin, and D. V. Skryabin, "Solitons and frequency combs in silica microring resonators: Interplay of the Raman and higher-order dispersion effects," *Phys. Rev. A*, vol. 92, 2015, Art. no. 033851.
- [62] V. E. Lobanov, A. V. Cherenkov, A. E. Shitikov, I. A. Bilenko, and M. L. Gorodetsky, "Dynamics of platicons due to third-order dispersion," *Eur. Phys. J. D*, vol. 71, pp. 1–5, 2017.
- [63] P. Parra-Rivas, S. Coulibaly, M. Clerc, and M. Tlidi, "Influence of stimulated Raman scattering on Kerr domain walls and localized structures," *Phys. Rev. A*, vol. 103, 2021, Art. no. 013507.